WATER RESOURCES RESEARCH, VOL. 28, NO. 1, PAGES 285–297, JANUARY 1992

Evaluation of Liquid and Vapor Water Flow in Desert Soils Based on Chlorine 36 and Tritium Tracers and Nonisothermal Flow Simulations

BRIDGET R. SCANLON

Bureau of Economic Geology, University of Texas at Austin

The distribution of anthropogenic ^{36}Cl and ^{3}H was used along with numerical flow simulations to evaluate the relative importance of liquid and vapor flow in the shallow unsaturated zone of an area within the Chihuahuan Desert of Texas. Chlorine 36 is nonvolatile and is restricted to liquid phase flow, whereas tritiated water is volatile and can move in both liquid and vapor phases. Tritium penetrated 1 m deeper than ^{36}Cl, although ^{3}H fallout occurred later than that of ^{36}Cl. Deeper penetration of ^{3}H relative to that of ^{36}Cl was attributed to enhanced downward movement of ^{3}H in the vapor phase. The moisture flux calculated from the $^{36}Cl/Cl$ peak at 0.5-m depth was 1.4 mm yr^{-1}, whereas that based on the ^{3}H peak at 1.4-m depth was 7 mm yr^{-1}. The difference in moisture fluxes between the two tracers suggests a vapor flux of approximately 6 mm yr^{-1}. The vapor flux hypothesis was tested using nonisothermal liquid and vapor flow simulations with the computer code SPLaSH-WaTr. Simulations of 5-day periods in the winter and summer were conducted to represent the extremes in temperature gradients. The calculated vapor flux was two to eight orders of magnitude greater than the liquid flux for the periods simulated. Predicted vapor fluxes were upward in the top 0.04 m of the unsaturated zone in the summer and winter in response to steep water potential gradients induced by surface evaporation. Below the evaporation front, from depths of 0.15 to 1 m, downward vapor fluxes in the summer were much greater than generally upward vapor fluxes in the winter. These results suggest an annual net downward vapor flux that is consistent with the chemical tracer data.

INTRODUCTION

Desert soils are increasingly being considered for waste disposal because low moisture fluxes characteristic of these systems retard contaminant transport. The relative magnitude of liquid and vapor flux is important in prediction of volatile and nonvolatile contaminant transport from waste disposal facilities in arid systems. Both chemical and physical data have been used to evaluate these fluxes; however, few studies combine both types of data to evaluate unsaturated flow processes.

Transport of ^{36}Cl and ^{3}H has been investigated in many previous studies; most were restricted to laboratory column experiments to evaluate solute transport parameters [*van Genuchten and Wierenga*, 1977; *Wierenga and van Genuchten*, 1989; *Wierenga et al.*, 1975]. The effects of artificial boundary conditions and of soil disturbance complicate the use of laboratory column studies to replicate field conditions. In addition, some studies have shown that solute transport parameters are scale dependent [*Wierenga and van Genuchten*, 1989], which limits extrapolation from laboratory to field scales. Most laboratory column experiments showed that ionic Cl or ^{36}Cl migrated faster than ^{3}H [*Biggar and Nielsen*, 1962; *Krupp et al.*, 1972; *Wierenga and van Genuchten*, 1989]. Faster penetration of Cl or ^{36}Cl was attributed to anion exclusion. Additional studies showed that anion exclusion occurred at high *p*H and anion adsorption at low *p*H [*Nielsen et al.*, 1986]. Faster migration of Cl relative to that of ^{3}H was also recorded in field tracer experiments [*Gvirtzman et al.*, 1986; *van de Pol et al.*, 1977]. Calculated anion velocities were as much as twice the estimated water velocities [*Gvirtzman et al.*, 1986; *James and Rubin*, 1986].

Paper number 91WR02200.
0043-1397/92/91WR-02200$05.00

More recent field studies in desert soils of New Mexico showed deeper penetration of ^{3}H relative to that of ^{36}Cl [*Phillips et al.*, 1988]. Various hypotheses, including chloride adsorption, salt sieving, and vapor transport of ^{3}H, were examined to explain the difference [*Phillips et al.*, 1988]. Laboratory experiments suggested that vapor transport was responsible [*Phillips et al.*, 1988]. Distribution of stable isotopes of hydrogen and oxygen at that site suggested that downward vapor transport in the summer may constitute a large part of the total flow in the upper meter of the unsaturated zone [*Knowlton*, 1990; *Knowlton et al.*, 1989].

Soil physics approaches also have been used to evaluate liquid and vapor fluxes in the shallow unsaturated zone. A field experiment was conducted to quantify liquid and vapor fluxes in the upper 0.15 m of the unsaturated zone for 6 days following saturation [*Rose*, 1968*a*, *b*]. Results from this study showed upward liquid fluxes throughout the 6 days, downward vapor fluxes during the daytime, and much lower upward vapor fluxes at night. Diurnal fluctuations in vapor flux resulted from diurnal variations in temperature gradients. Vapor flux was an order of magnitude greater than liquid flux at water potentials as high as −0.5 MPa. Another study investigated in detail water movement in response to diurnally varying atmospheric conditions in the top 0.1 m of the unsaturated zone after an irrigation event [*Jackson et al.*, 1973]. The evaporation rate at the soil surface was measured directly with a weighing lysimeter, and moisture flux was calculated at various depth intervals down to 0.09 m using the surface evaporation rate and changes in water content at these depths. The dynamic nature of water movement was demonstrated by variations in magnitude and direction of moisture flux as many as four times during a 24-hour period; however, the magnitudes of liquid and vapor fluxes were not separately quantified in the study. Numerical simulations of nonisothermal water flow in conjunction with a field exper-

iment were used to evaluate the effect of coupling heat and moisture flow equations [*Sophocleous*, 1979]. That study showed that temperature profiles were not noticeably affected by coupling but that subsurface moisture fluxes were. Although the model was used to calculate evaporation from dry soils, it did not include a detailed analysis of atmospheric forcing required to accurately simulate fluxes at the soil surface [*Sophocleous*, 1979]. The soil physics approach provides invaluable insight into liquid and vapor transport processes; however, the results from these studies are generally restricted to both the short time and the initial conditions considered in the experiments.

The objective of this study was to evaluate flow processes of the shallow unsaturated zone in a desert soil. Key components of the research included (1) evaluation of moisture flux from measurement of ^{36}Cl and ^{3}H in field samples, (2) estimation of solute transport parameters in the shallow unsaturated zone, (3) comparison of chemical tracer data at this site with that in other arid regions, and (4) comparison of the distributions of ^{36}Cl and ^{3}H with nonisothermal flow simulation results to evaluate the relative importance of liquid and vapor flow. Tritium and ^{36}Cl constitute long-term natural tracers. These tracers were used to estimate the net moisture flux in the shallow unsaturated zone, and to calculate solute transport parameters characteristic of the unsaturated zone, which avoids difficulties associated with the limited time and length scales of laboratory experiments. Although most previous studies of unsaturated flow focused on the use of either chemical or hydraulic methods to evaluate water movement in the unsaturated zone, detailed analysis of both chemical and hydraulic data should provide a more thorough understanding of unsaturated flow processes.

Anthropogenic Radioisotopes

The penetration depths of radioisotopes such as ^{36}Cl and ^{3}H can be used to estimate the moisture velocity by dividing the peak depth by the elapsed time since peak fallout. The moisture flux is calculated from the moisture velocity times the average volumetric moisture content above the peak depth. This method assumes steady state moisture content with depth; however, moisture content displays seasonal fluctuations. To avoid overestimation of moisture flux, soil samples should be collected after long dry periods. Chlorine 36 is nonvolatile and is restricted to liquid phase flow. The ^{36}Cl isotope has a half-life of $(3.01 \pm 0.04) \times 10^5$ years. Natural ^{36}Cl is produced by cosmic ray spallation of ^{40}Ar [*Bentley et al.*, 1986]. The ratio of natural ^{36}Cl to stable chloride ($^{36}Cl/Cl$), calculated using an atmospheric box model, is approximately 0.5×10^{-12} for this area [*Bentley et al.*, 1986]. Chlorine 36 was enriched in the atmosphere by neutron activation of ^{35}Cl in seawater by weapons tests conducted in the South Pacific between 1952 and 1958, with ^{36}Cl fallout peaking in 1955 [*Bentley et al.*, 1986]. Temporal variations in ^{36}Cl fallout were predicted on the basis of an atmospheric box model (Figure 1). Latitudinal variation in ^{36}Cl was evaluated using ^{185}W [see *Phillips et al.*, 1988, Figure 2] and indicates that the total ^{36}Cl fallout in the southwestern United States was approximately 3.4×10^{12} atoms m^{-2}.

Tritium has a half-life of 12.43 ± 0.05 years and is produced naturally by the interaction of ^{14}N with cosmic ray neutrons according to the following reaction [*International Atomic Energy Agency* (IAEA), 1983]:

$$^{14}_{7}N + {}^{1}_{0}n = {}^{12}_{6}C + {}^{3}_{1}H \quad (1)$$

Natural production is approximately 10 tritium units (1 TU is 1 ^{3}H atom in 10^{18} atoms of ^{1}H or 0.118 Bq kg^{-1}). Tritiated water is volatile and can move in both liquid and vapor phases. Bomb ^{3}H was produced initially in 1952, and peak production followed in 1963–1964. Tritium concentrations increased from 10 to ≥2000 TU during atmospheric nuclear testing [*IAEA*, 1983]. Temporal variations in average ^{3}H concentrations of precipitation for the northern hemisphere [*IAEA*, 1983] and for Socorro and Albuquerque, New Mexico [*Duval*, 1986] (Figure 1) should be representative of ^{3}H concentrations of precipitation in the Hueco Bolson (G. W. Gross, personal communication, 1989). The tritium input function for the study area was not estimated because it depends on time and intensity of precipitation and on evaporation rate which cannot be accurately evaluated.

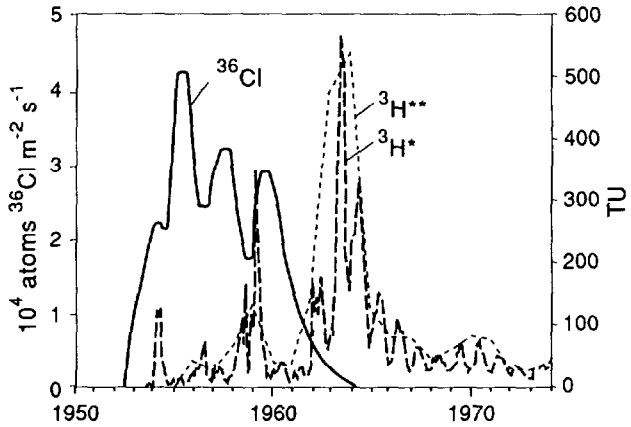

Fig. 1. Temporal variations in predicted bomb ^{36}Cl fallout between 30°N and 50°N latitude [*Bentley et al.*, 1986] and in ^{3}H fallout of precipitation for the northern hemisphere ($^{3}H^{*}$) [*IAEA*, 1983] and for Socorro (1956–1976) and Albuquerque (1977–1984), New Mexico ($^{3}H^{**}$) [*Duval*, 1986]; decay corrected to 1989.

Site Description

The study area (31°25'N, 105°40'W), approximately 65 km southeast of El Paso, lies within the Chihuahuan Desert of Texas in the Hueco Bolson, which is a 200-m-thick, sediment-filled basin. The unsaturated zone consists of 0 to 15 m of coarse-grained sediment, underlain by approximately 140 m of clay with interbedded silt and sand. Regional climate is subtropical arid [*Larkin and Bomar*, 1983]; long-term (1966–1987) mean annual precipitation is 280 mm and exhibits large interannual variations that range from 110 to 430 mm in Fort Hancock (16 km southwest of the study area). Approximately 60% of the precipitation falls between June 1 and September 30 as convective summer storms. Potential evapotranspiration (class A pan) is as much as seven times mean annual precipitation. Relatively flat topography (slopes ≤ 1%) and high-intensity storms generally result in sheet flow. Ephemeral streams drain the alluvial plain and flow into arroyos that border the study area. The streams and arroyos are generally dry except immediately after precipitation.

Physical Hydrology

The following general flow equation modified from *de Marsily* [1986] outlines the potential gradients that may be important in controlling unsaturated flow:

$$q = -L_1\nabla(\psi + \psi_z) - L_2\nabla T - L_3\nabla\psi_\pi \quad (2)$$

where ψ is matric potential, ψ_z is gravitational potential, T is temperature, ψ_π is osmotic potential, L_1, L_2, and L_3 are proportionality constants, and ∇ is a gradient operator. Total flux in the shallow unsaturated zone consists of liquid and vapor flux components. The direction of liquid flux is controlled primarily by water potential gradients and is negligibly affected by temperature gradients. In contrast, vapor flux consists of isothermal and thermal components. The direction of isothermal vapor flux is controlled by water potential gradients, and that of thermal vapor flux by temperature gradients.

Because hydrologic data will be compared with chemical tracer data, the major findings of the physical flow studies, detailed by *Scanlon et al.* [1991], are summarized here. Osmotic potential was estimated from chloride concentration data according to the van't Hoff equation [*Campbell*, 1985]. Osmotic potentials were small (0 to −0.8 MPa) and were neglected in the flow equation. Water (matric and osmotic) potential and temperature were measured with psychrometers. The terms "water potential" and "matric potential" are used interchangeably in this study because the osmotic component of water potential was generally less than 5%. All water potential profiles showed an increase in water potential with depth except in the shallow subsurface (0.2 m) immediately after precipitation. Laboratory-measured water potentials ranged from a minimum of −16 MPa at the soil surface to approximately −2 MPa at 15-m depth. The general increase in water potential with depth indicated that the driving force for liquid water and isothermal vapor movement was directed upward. In situ monitoring of water potential measured at depths of 0.3 to 15 m showed that water potentials were fairly uniform throughout the year. In contrast, soil temperature displayed large seasonal and diurnal fluctuations. Seasonal fluctuations were restricted to the upper 5 m of the unsaturated zone, whereas diurnal fluctuations primarily occurred in the upper 0.2 m. The amplitude of the temperature fluctuations decreased with depth, and the phase of the wave also shifted with depth. Summer temperatures generally decreased, whereas winter temperatures generally increased, with depth. Predominantly downward summer temperature gradients opposed upward water potential gradients and suggested a downward driving force for thermal vapor movement. Generally upward winter temperature gradients were similar to upward water potential gradients and indicated an upward driving force for thermal vapor flow.

METHODS

Chemical Tracers

Twenty-six samples were collected for ^{36}Cl analysis in an ephemeral stream setting in January 1989, because precipitation is lowest at this time. The sampling interval was predetermined from a chloride profile in a nearby borehole [*Scanlon et al.*, 1990]. The travel time (t) represented by chloride concentration at depth z was evaluated by dividing the total mass of soil water chloride (Cl_{sw}) from the surface to that depth by the chloride flux (J_s):

$$t = \sum Cl_{sw}\, z/J_s \quad (3)$$

The chloride flux into the soil was approximated by the chloride concentration in precipitation times the average annual precipitation [*Scanlon*, 1991]. The chloride data suggested that water had infiltrated to a depth of 0.5 m during the last 35 years. Samples for ^{36}Cl analysis were collected with a trowel at 0.1-m intervals down to a depth of 1 m in a pit and stored in plastic bags. The amount of soil required to obtain 20 mg of chloride was calculated from chloride concentration data and ranged from 10 kg near the surface to 1 kg at depth. Core samples were collected at 0.25-m increments from depths of 1 to 5 m with Shelby tubes in a hollow stem auger; samples were sealed in glass jars. Subsamples for moisture and chloride content were sealed in plastic cups. Twenty-six samples for ^3H analyses were collected adjacent to the ^{36}Cl sample location at the same depth intervals and by the same techniques used to collect samples for ^{36}Cl. The 1-kg soil mass required to obtain approximately 0.05 L of water for ^3H analyses was calculated from moisture content data from a nearby borehole. Samples for ^3H analysis were sealed in plastic bags.

The $^{36}Cl/Cl$ ratios were measured by tandem accelerator mass spectrometry (TAMS) at the University of Rochester (Rochester, New York) [*Elmore et al.*, 1979]. Laboratory preparation of ^{36}Cl samples for analysis followed procedures outlined by *Mattick et al.* [1987]. Double-deionized water was added, and the mixture was stirred with an electric stirrer for approximately 12 hours. AgCl was precipitated from the chloride solution by addition of $AgNO_3$. Because ^{36}S interferes with $^{36}Cl/Cl$ analysis, $Ba(NO_3)_2$ was added to the solution to precipitate $BaSO_4$. To evaluate chemical contamination during sample preparation, Weeks Island halite, which has a negligible $^{36}Cl/Cl$ ratio (0.05 to 2×10^{-15}), was subjected to the same purification procedure as the soil samples. The $^{36}Cl/Cl$ ratios from the Weeks Island halite blank were similar to those of the University of Rochester blank and indicated that no chemical contamination had occurred during sample processing. Uncertainties were calculated following *Elmore et al.* [1984] and are reported as one standard deviation.

Water for ^3H analysis was extracted from soil samples by azeotropic distillation with toluene [*Allison et al.*, 1985]. After distillation the water samples were purified of toluene by heating in paraffin wax. Tritium was determined by direct liquid scintillation at the University of Waterloo (Waterloo, Ontario, Canada). Although the analytical precision of direct liquid scintillation is low (±8 TU) compared with that of enriched ^3H methods (±0.8 TU), the former technique was chosen because of the small sample volume available and because traces of toluene in the water samples would cause problems with the enriched ^3H method.

Numerical Modeling of Nonisothermal Water Transport

Coupled water and heat flow was modeled with the computer code SPLaSHWaTr [*Milly and Eagleson*, 1980] to determine the relative importance of liquid and vapor transport in the upper 5 m of the unsaturated zone. SPLaSHWaTr

is an acronym for Simulation Program for Land Surface Heat and Water Transport. Matric potential (ψ) based equations derived from the moisture content (θ) based equations of *Philip and de Vries* [1957] are used in SPLaSHWaTr. The ψ-based approach is preferred over the θ-based approach because the former can be used to simulate water flow in layered soil systems, whereas the latter is restricted to homogeneous soil systems. Water (matric and osmotic) potential rather than matric potential was measured at the site; however, the osmotic potential, calculated from chloride concentration data, is generally less than 5% of the water potential [*Scanlon et al.*, 1991].

Governing equations. The total mass flux (q_m) consists of the following components:

$$q_m/\rho_l = q_l/\rho_l + q_v/\rho_l \tag{4}$$

where q_l is liquid flux, q_v is vapor flux, and ρ_l is liquid density. Darcy's law describes the liquid flux. Liquid flux occurs in response to matric potential and temperature gradients. The temperature dependence of matric potential is shown by the following equation [*Milly*, 1984]:

$$\Psi = \psi \exp\left[-C_\psi (T - T_0)\right] \tag{5}$$

where

$$C_\psi = \frac{1}{\psi}\frac{\partial \psi}{\partial T}\bigg|_\theta$$

T is temperature, T_0 is an arbitrary reference temperature, and θ is moisture content. A value of 6.8×10^{-3} °K^{-1} was assigned to C_ψ in SPLaSHWaTr [*Milly*, 1984], which is approximately three times the value predicted by the surface tension model of *Philip and de Vries* [1957]. The surface tension model generally underestimates thermally induced liquid flow [*Wilkinson and Klute*, 1962]; therefore, this value should provide a better approximation of that flow. The temperature dependence of the hydraulic conductivity (K) is given by

$$K = K_s K_r(\theta)\nu(T_0)/\nu(T) \tag{6}$$

where K_s is saturated hydraulic conductivity at the reference temperature T_0, K_r is relative hydraulic conductivity, which is a function of moisture content (θ), and ν is kinematic viscosity [*Milly*, 1984].

The vapor flux is given by

$$q_v/\rho_l = q_{iv} + q_{Tv} = -D_{\psi v}\nabla\psi - D_{Tv}\nabla T \tag{7}$$

where q_{iv} is isothermal vapor flux, q_{Tv} is thermal vapor flux, $D_{\psi v}$ is isothermal vapor diffusivity, $\nabla\psi$ is matric potential gradient, D_{Tv} is thermal vapor diffusivity, and ∇T is overall average temperature gradient. $D_{\psi v}$ and D_{Tv} are given by *Milly* [1982] and *Milly and Eagleson* [1980].

The following equation was used to solve for the heat flux [*Milly*, 1982]:

$$q_h = -\lambda\nabla T - \rho_l L D_{\psi v}\nabla\psi + c_l(T - T_0)q_m \tag{8}$$

where q_h is vertical heat flux, λ is effective thermal conductivity of the bulk medium, L is latent heat of vaporization of water vapor, c_l is specific heat of liquid water, and T_0 is the datum for zero enthalpy. The effective thermal conductivity was calculated according to the method of *de Vries* [1963] [*Milly*, 1984].

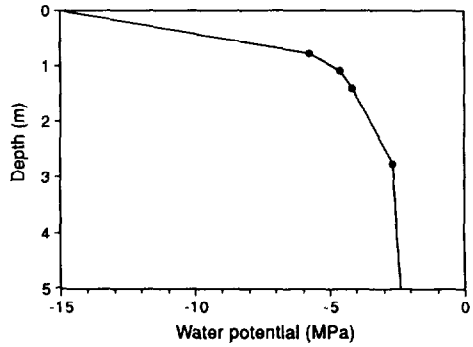

Fig. 2. Water potential variations with depth measured on January 17, 1990.

SPLaSHWaTr uses the Galerkin finite element method to solve the one-dimensional form of the governing partial differential heat flow and moisture flow equations. The time derivative is approximated by a fully implicit, backward finite difference scheme. An automatic time-stepping procedure is used in which the time step size is controlled such that the absolute changes in moisture content, water potential, and temperature are less than those that are specified in the input data. The code was implemented on a MicroVax computer workstation.

Model Input. Liquid and vapor flux in response to diurnally varying environmental conditions was simulated for the summer and winter periods in the upper 5 m of bare soil to assess the net movement of water vapor on an annual basis. Field measurements provide initial and boundary conditions for the model and also validate its results. Data from June 17, 1990, and January 17, 1990, were chosen to represent the extremes in soil temperature gradients [*Scanlon et al.*, 1991] and because they correspond to periods when hourly soil temperatures and water potentials were recorded by the in situ psychrometers. Initial conditions consisted of the distribution of water potential and soil temperature with depth. In the shallow subsurface (≤0.8 m) water potentials were out of range of the in situ psychrometers (≤−8 MPa); therefore, the surface water potential was assigned a value of −15 MPa, which is approximately equal to the lowest measured water potential by the laboratory psychrometer (Figure 2). The temperature at the soil surface was approximated by the soil temperature measured at 0.01 m depth. Nodal values of initial water potentials and temperatures were obtained by linearly interpolating observed values. Input parameters to describe the upper boundary condition consist of hourly averages of air temperature, solar radiation, wind speed, and absolute humidity (Figure 3) that were measured at 2 m above the soil surface in a meteorologic station approximately 0.5 km from the subsurface test plots. Incoming longwave radiation was calculated according to *Milly and Eagleson* [1982]. June temperatures were 14° to 23°C higher than January temperatures. Incoming solar and longwave radiation was higher in June than in January. Solar radiation was highest during the daytime and zero at night. In contrast, incoming longwave radiation was relatively uniform throughout the 24-hour period. Absolute humidity also showed diurnal and seasonal fluctuations

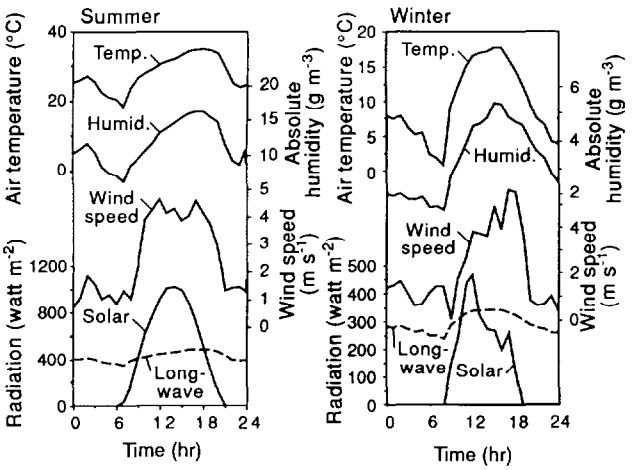

Fig. 3. Variations in observed solar radiation, calculated longwave radiation, and observed air temperature, wind speed, and absolute humidity at 2 m above ground surface on (*a*) June 17, 1990, and (*b*) January 17, 1990.

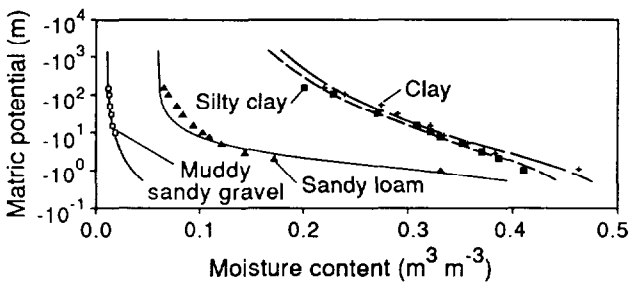

Fig. 4. Retention curves for different soil textures. Points represent measured matric potentials and moisture contents and lines represent fitted retention curves based on *van Genuchten* [1980]. Sediment samples that contained gravel were classified according to *Folk* [1974] and those that lack gravel were classified according to the *U.S. Department of Agriculture* [1975].

similar to variations in air temperature. Wind speeds were highest during the daytime and lowest at night. January and June wind speed data were similar. Information on albedo for dry (0.2) and wet (0.1) silt loam was obtained from *Milly and Eagleson* [1982]. Boundary conditions at the base of the modeled region consisted of constant water potential and temperature fixed at ambient values. The 24-hour atmospheric forcing was repeated five times to establish dynamic equilibrium. Approximately 40 elements were used to represent the upper 5 m of the unsaturated zone. Small nodal spacing (≥0.25 mm) was employed near the soil surface, where temperature and water potential change rapidly, whereas larger nodal spacing (≤500 mm) was used at depth.

Soil texture for the model was based on grain-size analyses of soil samples from the same borehole that yielded chloride profile data. The percent quartz, mineral, and organic matter were input for soil thermal conductivity calculations. Material properties were assigned on the basis of laboratory retention data for similar soil textures that ranged from silty clay from the surface to 0.35 m depth, clay to 1.3 m depth, and muddy sand gravel down to 5 m depth (Figures 4 and 5, appendix[1] Table A1) [*Scanlon et al.*, 1991]. Information on the retention functions between moisture content and water potential for different soil textures (Figure 4) was based on analytical expressions [*van Genuchten*, 1980]. Hysteresis was neglected because only monotonic drying problems were simulated. Unsaturated hydraulic conductivity was estimated from the fitted soil water retention curves and the measured K_s data following *Mualem* [1976]. The temperature dependencies of model-calculated hydraulic conductivity (K) and isothermal ($D_{\psi v}$) and thermal (D_{Tv}) vapor diffusivity for clay and muddy sandy gravel are shown in Figure 5.

The time step size is controlled such that temperature variations are less than 0.1°C or moisture content variations are less than 0.001 m^3 m^{-3}. Moisture content rather than matric potential was chosen to control the time step size because large variations in matric potential can occur in very dry systems with little change in moisture content, as reflected in moisture retention curves (Figure 4).

Results and Discussion

Chemical Tracers

The $^{36}Cl/Cl$ profile from an ephemeral stream setting includes a well-defined peak of 6.6×10^{-12} at 0.5-m depth (Figure 6, Table 1) which is approximately equal to the depth of the center of mass of the ^{36}Cl concentration (0.6 m). A background ratio of 0.47×10^{-12} below 1.25 m agrees with

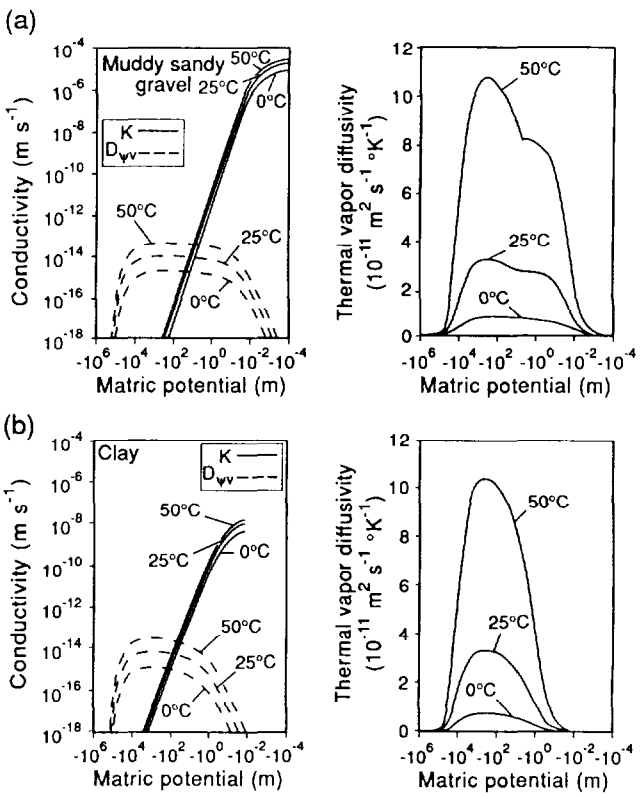

Fig. 5. (*a*) Liquid hydraulic conductivity (K) and isothermal vapor diffusivity ($D_{\psi v}$) and (*b*) thermal (D_{Tv}) vapor diffusivity as a function of water potential and temperature for different soil textures.

[1]The appendix tables are available with entire article on microfiche. Order from American Geophysical Union, 2000 Florida Avenue, N.W., Washington, D. C. 20009. Document W91-006; $2.50. Payment must accompany order.

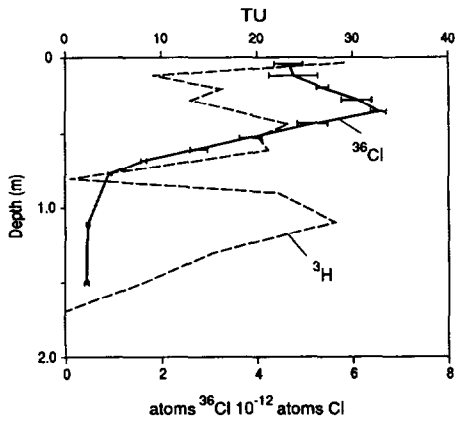

Fig. 6. Vertical profile in ^{36}Cl/Cl ratios and ^{3}H concentrations. The bars represent 1 standard deviation in the ^{36}Cl/Cl ratios. The analytical uncertainty associated with the ^{3}H measurements is ±8 TU and was omitted for clarity.

the predicted natural fallout of 0.5×10^{-12} for this latitude [*Bentley et al.*, 1986]. The total inventory of bomb ^{36}Cl is 2.5×10^{12} atoms m^{-2} from the sampled borehole, which is 74% of the predicted fallout at this latitude (3.4×10^{12} atoms m^{-2}) [*Phillips et al.*, 1988]. The average moisture velocity calculated from the depth of the ^{36}Cl/Cl peak (0.5 m) and the time since peak fallout (35 years) is 14 mm yr^{-1}. Calculated moisture flux is 1.4 mm yr^{-1} for the past 35 years, based on an average volumetric moisture content of 0.10 m^3 m^{-3} in the upper 0.5 m of the unsaturated zone. This flux represents 0.5% of the mean annual precipitation rate in the region. The depth of the ^{36}Cl/Cl peak was used instead of the maximum depth of the ^{36}Cl/Cl penetration (i.e., above background) because piston-type flow is assumed, and spreading around the peak is attributed to hydrodynamic dispersion. Although moisture flux is expressed on an annual basis for comparison with other tracers, actual percolation in these desert soils is episodic.

The ^{3}H profile consists of three peaks that are of approximately equal magnitude (23 to 29 TU) (Figure 6, Table 1). The existence of discrete peaks suggests very little mixing between percolation events. If piston-type flow is assumed, the shallowest peak should represent recent precipitation, whereas the deepest peak should represent the 1963–1964 bomb pulse. Although the 1963–1964 peak would be expected to be much greater than the other peaks on the basis of ^{3}H fallout, sample contamination appears unlikely because samples from the same depth intervals in a nearby borehole yielded similar results. A moisture velocity of 56 mm yr^{-1} was calculated by assuming that the peak at 1.4-m depth represents 1963–1964 percolation and the time since peak fallout was 25 years. The corresponding moisture flux was 7 mm yr^{-1}, based on the average volumetric moisture content in this zone of 0.13 m^3 m^{-3}. Moisture flux calculated from the ^{3}H data is much higher than that based on the ^{36}Cl/Cl peak (Figure 6) because ^{3}H penetrated deeper than ^{36}Cl, although peak ^{3}H fallout occurred approximately 8 years later than that of ^{36}Cl (Figure 1). At 0.9- to 1-m depth, ^{3}H concentrations were below the detection limit. At a moisture flux of 7 mm yr^{-1}, this low ^{3}H level corresponds to influx of water between 1971 and 1973 and may reflect below normal precipitation during this period and/or loss of ^{3}H by

TABLE 1. Soil Texture, Volumetric Moisture Content, Chloride Concentration, Chloride Mass Balance Age, Chloride Moisture Flux, ^{36}Cl/Cl Ratios, and ^{36}Cl and ^{3}H Concentrations

Depth, m	Soil Texture	Moisture Content, m^3 m^{-3}	Chloride per Cubic Meter Soil Solution, g Cl$^-$	Chloride Mass Balance Age, yr	Chloride Moisture Flux, mm yr^{-1}	Ratio of Atoms ^{36}Cl to Atoms Cl, $\times 10^{-12}$	Atoms of Bomb ^{36}Cl per Cubic Meter of Soil, $\times 10^{12}$	Tritium, TU (±8)
0.0 – 0.1	loam	0.05	74.0	2	1.10	4.64 ± 0.29	0.28	29
0.1 – 0.2	loam	0.11	115.2	18	0.70	4.77 ± 0.26	0.90	9
0.2 – 0.3	loam	0.12	224.1	50	0.36	5.37 ± 0.06	2.15	16
0.3 – 0.4	clay loam	0.12	165.0	74	0.49	6.10 ± 0.16	1.88	13
0.4 – 0.5	clay loam	0.12	289.3	117	0.28	6.56 ± 0.08	3.60	18
0.5 – 0.6	clay loam	0.13	405.2	181	0.20	5.18 ± 0.15	4.14	23
0.6 – 0.7	silty clay loam	0.13	612.1	277	0.13	3.93 ± 0.24	4.53	20
0.7 – 0.8	clay loam	0.13	759.8	399	0.11	2.82 ± 0.17	3.90	21
0.8 – 0.9	silty clay loam	0.13	934.2	550	0.09	1.63 ± 0.49	2.35	15
0.9 – 1.0	clay	0.15	1193.5	769	0.07	0.93 ± 0.38	1.30	0
1.0 – 1.25	...	0.16	1473.6	1266	0.06	...	...	22
1.25 – 1.50	...	0.15	2174.5	2256	0.04	0.47 ± 0.21	−0.19	28
1.50 – 1.75	...	0.15	2579.7	3468	0.03	...	...	15
1.75 – 2.00	...	0.08	2168.7	4015	0.04	0.46 ± 0.23	−1.21	8
2.00 – 2.25	gravelly muddy sand	0.09	2276.0	4612	0.04	...	...	0

Three dots indicate no data.

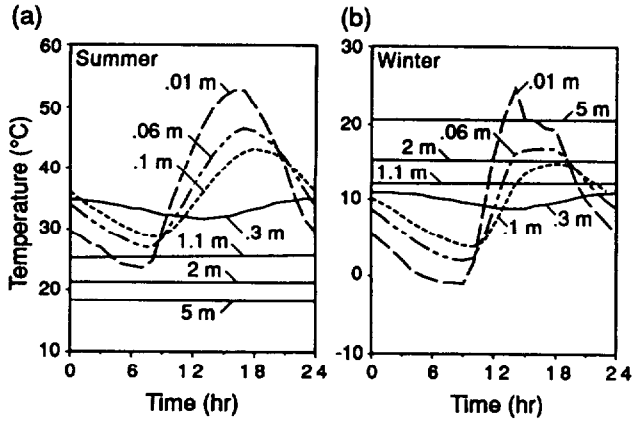

Fig. 7. Diurnal variations in predicted soil temperatures for (*a*) June 17, 1990, and (*b*) January 17, 1990.

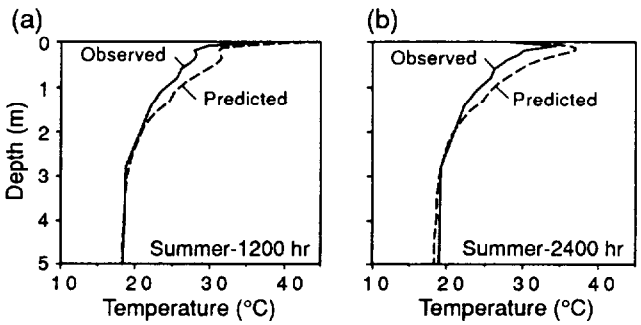

Fig. 8. Comparison of observed and predicted soil temperatures for (*a*) 1200 hours and (*b*) 2400 hours on June 17, 1990.

evapotranspiration; however, climatic data are not available for the study area for this time.

The ^{36}Cl/Cl profile was compared with the ionic chloride profile (Table 1). The time represented by chloride concentration at each depth interval was calculated according to (3). The chloride age data underestimate the position of the ^{36}Cl/Cl peak by approximately 0.2 m. The average moisture flux based on chloride mass balance (0.9 mm yr^{-1}) for a similar time is slightly lower than that calculated from the ^{36}Cl/Cl peak (1.4 mm yr^{-1}).

Comparison of Hydraulic and Chemical Approaches

The chemical tracer data were compared with hydraulic data [*Scanlon et al.*, 1991] to evaluate controls on flow in the unsaturated zone. Water potential data suggest an upward driving force for liquid water movement, except in the shallow subsurface immediately after precipitation. This upward force contrasts with the cumulative, downward directed flux indicated by the environmental tracer data. If upward liquid water movement occurred, the highest ^{36}Cl/Cl ratios and Cl concentrations should be at land surface; however, the maximum ^{36}Cl/Cl ratio is at a depth of 0.5 m and maximum Cl concentrations are at depths of 3.5 to 6.5 m [*Scanlon*, 1991].

The diffusion equation was used to determine if diffusion alone could account for the distribution of the environmental tracers, using ^{36}Cl as an example. The one-dimensional diffusion equation to be solved is

$$D_e(\partial^2 c/\partial z^2) = \partial c/\partial t \qquad (9)$$

The effective diffusion coefficient (D_e) for chloride is the product of the chloride diffusion coefficient in water times a transmission factor that includes the effects of tortuosity and increased viscosity of water in a porous medium relative to free water. D_e was estimated from laboratory data by *Porter et al.* [1960] to be 1.4×10^{-3} m^2 yr^{-1} and is within the range of estimated D_e values based on more recent studies by *Conca and Wright* [1991]. As an initial condition, ^{36}Cl was assumed to be uniformly distributed in the upper 0.2 m of the soil zone, the maximum penetration depth of the wetting fronts observed during the monitoring period. The following Laplace analysis of the diffusion equation [*Carslaw and Jaeger*, 1959] was used to solve for ^{36}Cl concentrations for an infinite soil column:

$$c = 0.5c_0\{\text{erf}\,[(a - z)/2(D_e t)^{1/2}] + \text{erf}\,[(a + z)/2(D_e t)^{1/2}]\} \qquad (10)$$

where c_0 is the initial concentration of 12.4×10^{12} atoms ^{36}Cl m^{-3} soil in the upper 0.2 m ($a = 0.2$), and $t = 35$ years. The ^{36}Cl profile calculated by diffusion is characterized by maximum ^{36}Cl concentration at land surface and cannot reproduce the observed ^{36}Cl concentration peak at a depth of 0.7 m (Table 1). This comparison suggests that advective flow must also be involved in producing the observed ^{36}Cl profile.

The discrepancy between the radioisotopic tracer data and the hydraulic data probably results in part from the limited time (~2 years) represented by the soil physics monitoring. The chemical tracers recorded moisture flux over a much longer (up to 35 years) time. In addition, the complexity of flow processes in the shallow unsaturated zone with repeated cycles of episodic infiltration and evapotranspiration may not be adequately represented by the hydraulic data, whereas the chemical tracers record the net flux. The radioisotopic tracers have only moved to depths of up to 2 m; therefore, the magnitude of the moisture flux in deeper sections of the unsaturated zone cannot be estimated from these tracers. Results of the ^{36}Cl and chloride mass balance methods are similar for the top 0.5 m and suggest that the downward movement of water should continue at least through the uppermost 20 m of the unsaturated zone [*Scanlon*, 1991]. Comparisons between the chloride mass balance data and the hydraulic data are difficult because of the many assumptions associated with the chloride mass balance method.

Movement of ^{36}Cl and Cl is restricted to liquid phase flow; however, ^{3}H can move in both liquid and vapor phases. The discrepancy between ^{36}Cl and ^{3}H transport in the Hueco Bolson may result from retardation of ^{36}Cl, acceleration of ^{3}H, or a combination of both. Possible retardation mechanisms for ^{36}Cl include anion adsorption and salt sieving [*Phillips et al.*, 1988]. Anion adsorption is unlikely because soils in the Hueco Bolson are basic and anion adsorption is uncharacteristic of basic soils. Salt sieving occurs when the water film thickness is less than that of the anion exclusion layer of the grain surfaces; however, information on salt sieving is generally restricted to laboratory data for saturated clays [*Nielsen et al.*, 1972]. Moisture contents in the ^{36}Cl soil

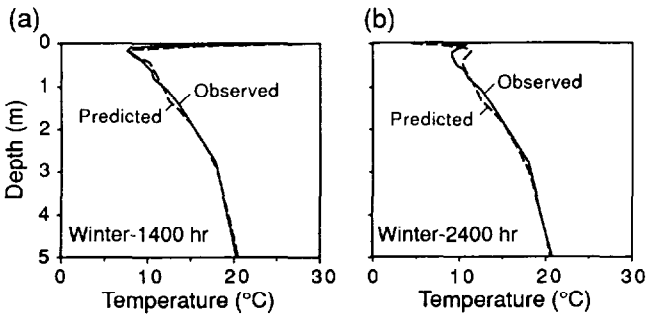

Fig. 9. Comparison of observed and predicted soil temperatures for (*a*) 1400 hours and (*b*) 2400 hours on January 17, 1990. Soil temperatures could not be compared at 1200 hours because they were not monitored at this time.

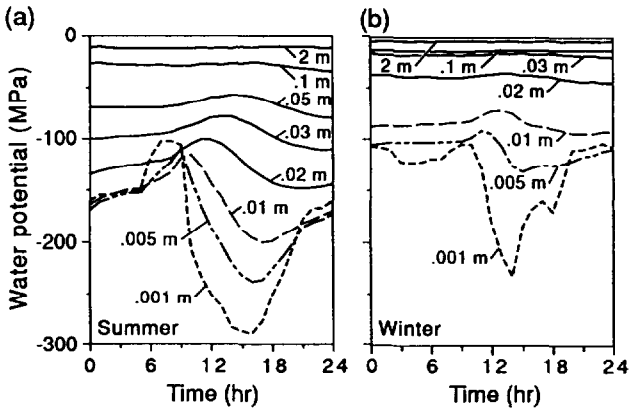

Fig. 10. Diurnal variations in predicted water potentials on (*a*) June 17, 1990, and (*b*) January 17, 1990.

samples are probably too great for salt sieving to be effective. The deeper penetration of ^{3}H relative to that of ^{36}Cl is more likely the result of enhanced downward movement of ^{3}H in the vapor phase. Differences in moisture fluxes between the two tracers suggest a downward vapor flux of ~6 mm yr^{-1}.

To determine if vapor diffusion could account for the discrepancy between moisture fluxes based on ^{36}Cl and those based on ^{3}H, liquid and vapor movement in response to water potential and temperature gradients was simulated for the shallow unsaturated zone according to procedures outlined in the methods section.

Numerical Simulations of Liquid and Vapor Flux

Output from the SPLaSHWaTr code consists of spatial and temporal variations in soil temperature, water potential, and moisture fluxes including liquid, and isothermal and thermal vapor flux. Cumulative mass balance errors for the 5-day simulation period were less than 1 part in 10^{6}, and energy balance errors were less than 1 part in 10^{2}. The CPU time required for the 5-day simulation was ~1 hour on the MicroVax station. Although 5 days were simulated for the winter and summer, little variation was observed between output for the first and fifth day; therefore, output from the model is shown for the last 24-hour period. Soil temperatures predicted by simulating transient flow in response to diurnal variations in meteorologic parameters (Figure 7) were compared with the observed soil temperatures (Figures 8 and 9). The surface roughness parameter that gave the best fit between observed and predicted soil temperature was 25 mm, which is a reasonable value for bare soil found in the area. Predicted summer temperatures decreased with depth during the day and increased slightly from the surface to 0.3 m and decreased from 0.3 m to 5 m at night (Figure 7*a*). Similar trends were found in observed temperature data. Predicted soil temperatures were lower than observed temperatures in the top 0.05 m and higher than observed temperatures from 0.05 to 1.5 m at 1200 hours (Figure 8*a*). At 2400 hours, predicted and observed soil temperatures were similar in the top 0.06 m, and predicted temperatures were higher than observed temperatures from 0.06 to 1.5 m depth (Figure 8*b*). Below 1.5 m, good agreement was found between observed and predicted soil temperatures throughout the 24-hour period.

Predicted winter temperatures decreased from the surface to 0.3 m and increased from 0.3 to 5 m during the day, whereas temperatures increased from the surface to 5 m depth at night (Figure 7*b*). These soil temperature gradients are similar to observed temperature gradients. Good agreement was found between observed and predicted soil temperatures at 1400 hours (Figure 9*a*); predicted soil temperatures were lower than observed temperatures from the surface to 0.1 m depth and higher than observed temperatures from 0.1 to 0.5 m depth at 2400 hours (Figure 9*b*). Absolute temperatures in winter were 0° to 35°C lower than those recorded in summer.

Diurnal fluctuations in water potentials were also predicted for the top 0.01 m of the soil during the summer (Figure 10*a*). Water potentials in this zone were lowest at approximately 1600 hours, which indicates that sediments were driest at this time. Water potential gradients in surficial sediments were steepest at this time also. Predicted water potentials in the shallow section ranged from −50 to −300 MPa, which is out of range of the in situ psychrometers (0 to −8 MPa). The range of predicted water potentials is consistent with water potentials (~−200 to −250 MPa) of surficial sediments at the Hanford site in Washington that were measured using a water activity meter [*Gee et al.*, 1990]. Observed and predicted water potentials at 1- to 2-m depth were in good agreement, and predicted water potentials did not vary much from the initial conditions. Similar patterns in predicted water potential variations were observed during the winter. Higher predicted water potentials in winter (Figure 10*b*) relative to those predicted for summer (Figure 10*a*) were attributed to lower evaporation rates in winter. The cumulative evaporation rate for the 5-day period was 0.6 mm in winter and 1.2 mm for the summer.

The sign convention for fluxes is that negative fluxes are downward and positive fluxes are upward. Liquid and vapor fluxes were plotted for the last 24-hour period of the simulation. Results for the upper 2 m of the unsaturated zone are shown because this represents the depth of soil most affected by diurnal variations in temperature and water potential. Data for the summer period showed a large predicted upward isothermal vapor flux during the day in the top 0.06 m, whereas isothermal vapor fluxes were smaller at night (Figure 11*a*). Isothermal vapor fluxes at 0.07 m and below were negligible and showed no diurnal fluctuations in magnitude or direction. This was consistent with predicted water po-

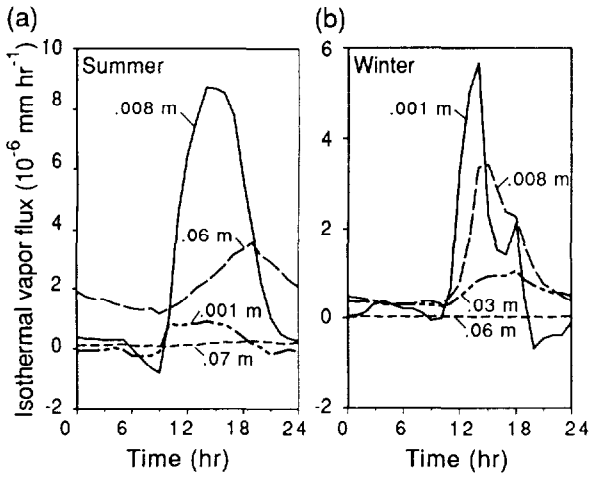

Fig. 11. Diurnal variations in predicted isothermal vapor flux (q_{iv}) on (*a*) June 17, 1990, and (*b*) January 17, 1990. Fluxes at depths of 0.07 m and 2 m are coincident in the summer and at depths of 0.06 m and 2 m are coincident in the winter.

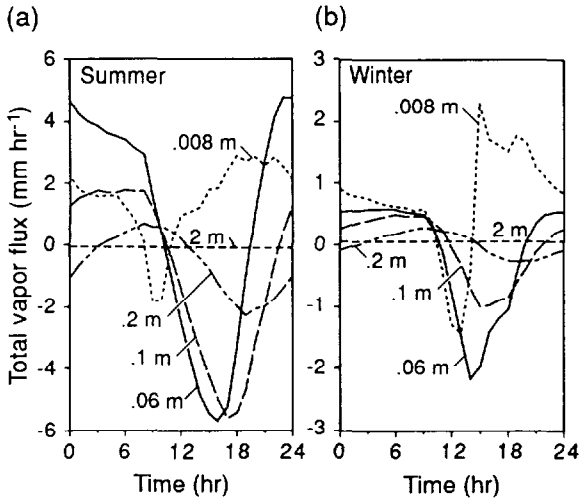

Fig. 13. Diurnal variations in predicted total vapor flux (q_{iv} + q_{Tv}) on (*a*) June 17, 1990, and (*b*) January 17, 1990.

tentials (Figure 10*a*), which showed steepest upward gradients during the day in the top 0.05 m depth and relatively uniform gradients below 0.05 m depth. Similar trends were found in the winter data (Figure 11*b*), but the upward fluxes were lower because of the lower predicted water potential gradients.

Predicted thermal vapor fluxes were downward during the day in summer and slightly upward at night (Figure 12*a*). The large downward fluxes during the day correspond to steep temperature gradients during this time (Figure 7*a*). Downward thermal vapor fluxes in winter (Figure 12*b*) are much lower than those calculated for summer because absolute soil temperatures in winter are as much as 35°C lower; temperature gradients are also lower than those measured during the summer (Figure 7). Total (or net) vapor flux (q_{iv} + q_{Tv}) is downward during the day and upward at night (Figure 13), similar to the trend in thermal vapor flux (Figure 12). The amplitude of the diurnal variations in total vapor flux decreases with depth, and flux is relatively uniform at 2 m.

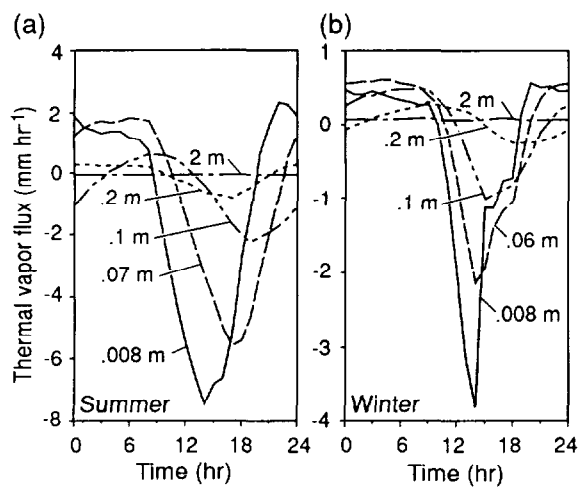

Fig. 12. Diurnal variations in predicted thermal vapor flux (q_{Tv}) on (*a*) June 17, 1990, and (*b*) January 17, 1990.

Net liquid flux estimated for the 5-day simulation period is two to eight orders of magnitude less than net vapor flux in summer and winter (Figure 14*a*). The greatest difference between liquid and vapor flux occurs in the top 1 m. Net vapor fluxes estimated for the summer 5-day simulation period are upward in the top 0.04 m of the soil zone and are downward throughout the remainder of the profile. In winter, net vapor fluxes are upward from the surface to 0.04 m and from 0.2 to 2 m, and are downward from 0.04 to 0.2 m. Although temperature gradients are steepest near the soil surface, upward isothermal vapor flux is much greater than downward thermal vapor flux in the top 0.04 m because steep water potential gradients are induced by surface evaporation. Below 1 m depth, downward vapor flux in summer is balanced by upward vapor flux in winter; net vapor flux on an annual basis should be negligible. Downward summer vapor fluxes from 0.15- to 1-m depth are 5 to 250 times greater than winter vapor fluxes; on an annual basis, this suggests a net downward vapor flux below the evaporation

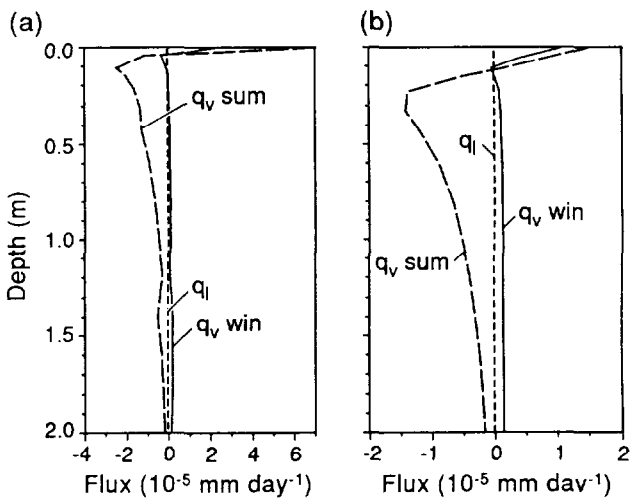

Fig. 14. Net vapor (q_v) and liquid (q_l) flux calculated for 5-day simulation period for June 17, 1990 (sum), and January 17, 1990 (win), for (*a*) a layered soil system and (*b*) a uniform sandy loam. Plots of liquid fluxes for June and January are coincident.

front. The net downward vapor flux is consistent with the chemical tracer data, which suggests that deeper penetration of ^{3}H relative to that of ^{36}Cl results from enhanced downward movement of ^{3}H in the vapor phase.

Sensitivity analyses were conducted to evaluate the effect of varying selected parameters on predicted water potentials, temperatures, and fluxes. Increases and decreases in the grid size by 50% did not alter the output. Changes in the lower boundary condition from constant temperature and constant water potential at ambient conditions to zero temperature and zero water potential gradients did not vary the predicted water potential or temperature profiles. Water movement in a homogeneous soil system was simulated to determine the effect of soil layering on liquid and vapor fluxes. Results from the layered system have previously been described. The homogeneous system was represented by uniform sandy loam (Figure 4). Although the maximum difference in predicted soil temperatures was only 2°C, predicted water potentials were up to −130 MPa lower in the top 0.1 m in the homogeneous system relative to the nonhomogeneous system. As a result of the differences in water potential and hydraulic conductivity, calculated isothermal vapor fluxes were 1 to 17 times higher in the top 0.2 m in the uniform soil relative to the layered soil (Figure 14).

Solute Transport Parameters

As shown earlier, diffusion alone cannot explain the distribution of ^{36}Cl; therefore, advective flow is also involved. Chlorine 36 may also be dispersed as it moves down through the soil profile. The following advection-dispersion equation is used to describe solute transport:

$$D(\partial^2 c/\partial z^2) - v(\partial c/\partial z) = \partial c/\partial t \qquad (11)$$

where D is the hydrodynamic dispersion coefficient and v is pore water velocity. Mechanical dispersion (D_m) and molecular diffusion (D^*) constitute hydrodynamic dispersion (D):

$$D = D_m + D^* \qquad (12)$$

At low flow velocities, the diffusive component (D^*) of the hydrodynamic dispersion coefficient may be dominant. The mechanical dispersion coefficient (D_m) is linearly related to pore water velocity for relatively homogeneous systems, the correlation coefficient being the dispersivity [*Wierenga and van Genuchten*, 1989]. Dispersivities based on laboratory columns (≤0.3 m length) are generally less than 0.01 m. Recent studies showed that dispersivities increased from 0.01 to 0.05 m as the soil column length increased from 0.3 to 6 m [*Wierenga and van Genuchten*, 1989]. This increase in dispersivity with scale is similar to that found in saturated zone studies and emphasizes the problem of extrapolating solute transport parameters from different scales.

The ^{36}Cl profile provides information on dispersion characteristics for the shallow unsaturated zone in the Hueco Bolson. An analytical solution of the one-dimensional advection-dispersion equation (equation (11)) [*van Genuchten and Alves*, 1982] was used as a model of the ^{36}Cl profile. Although flow in the shallow unsaturated zone is much more complex than suggested by this equation, which assumes unidirectional water movement with uniform velocity, more complex models were not used because detailed information

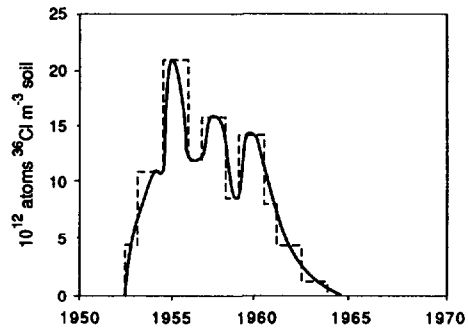

Fig. 15. Approximation of the ^{36}Cl fallout with a step function that was used in the analysis of advection-dispersion transport of ^{36}Cl.

for the past 35 years on spatial and temporal variations in flow directions, and velocities required for their solution, were unavailable. A uniform downward moisture velocity of 22 mm yr^{-1} was used on the basis of the depth of the peak ^{36}Cl concentration. The computer program of the analytical solution was modified to allow pulsed input of the ^{36}Cl concentrations. Only 73% of the predicted bomb fallout ratio was recovered at the site; therefore, the fallout was reduced by this amount as input for the model. The $^{36}Cl/Cl$ fallout ratio was converted to ^{36}Cl concentrations and was approximated with a step function (Figure 15). An initial estimate of the hydrodynamic dispersion coefficient was modified to obtain the best fit between the predicted and the observed ^{36}Cl concentrations. A hydrodynamic dispersion coefficient of 1.0×10^{-3} m^2 yr^{-1} was used in the final simulation (Figure 16). The goodness of fit of the calculated to the observed ^{36}Cl concentrations is indicated by a regression slope of 1 and an r^2 of 0.9. This hydrodynamic dispersion coefficient is similar to the previously estimated effective diffusion coefficient of 1.4×10^{-3} m^2 yr^{-1}. Because the hydrodynamic dispersion coefficient includes the effects of both mechanical mixing and molecular diffusion, this calculated dispersion coefficient indicates a low degree of mechanical mixing in this system. Even if a 50% uncertainty is assumed in the transmission coefficient used to calculate the effective diffusion coefficient, the hydrodynamic dispersion coefficient is within a factor of 1.5 of the effective diffusion coefficient. The similarity between the hydrodynamic dispersion coefficient and the effective diffusion coefficient indicates that concentration-driven diffusion can explain the

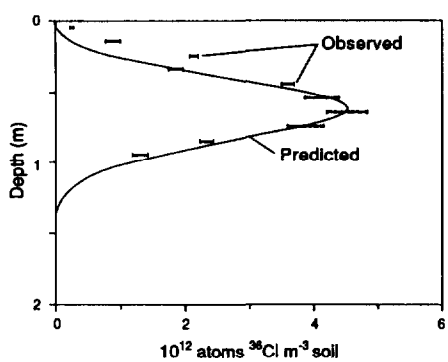

Fig. 16. Comparison of the calculated ^{36}Cl profile based on an analytical solution of the advection-dispersion equation and the observed ^{36}Cl profile.

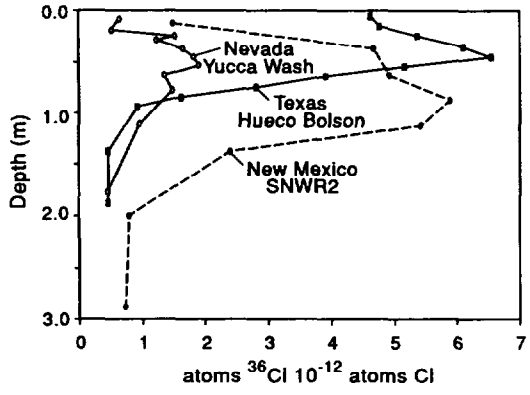

Fig. 17. Comparison of ^{36}Cl/Cl profiles sampled in Texas, New Mexico [*Phillips et al.*, 1988], and Nevada [*Norris et al.*, 1987].

broadening of the ^{36}Cl pulse. The low calculated dispersion coefficient probably results from the low water velocities and from alternating upward (evapotranspiration) and downward (infiltration) movement of water, which minimizes spreading of the tracer. The calculated hydrodynamic dispersion coefficient can be used to evaluate transport of anionic contaminants in the shallow unsaturated zone for similar time and length scales.

Comparison of Hueco Bolson Chemical Tracer Data With Data From Other Regions

Results of tracer studies conducted at the Hueco Bolson were compared with those from other regions to elucidate the environmental controls on water flow in desert soils. Three sites in central New Mexico were compared. Mean annual precipitation at the three sites studied in New Mexico (NMSUR (230 mm) and SNWR1 and SNWR2 (200 mm) [*Phillips et al.*, 1988]) is similar to that found at the Hueco Bolson (280 mm; Table A2). The total inventory of ^{36}Cl at the Hueco Bolson (2.5×10^{12} atoms ^{36}Cl m^{-2}) is the same as that measured at NMSUR but is approximately three times higher than that recorded at the SNWR sites in New Mexico (0.7×10^{12} to 0.9×10^{12} atoms ^{36}Cl m^{-2}). These differences in total inventories may represent local variations in ^{36}Cl fallout. Moisture flux based on the ^{36}Cl/Cl data from the Hueco Bolson can be directly compared with that from the SNWR2 site in New Mexico; however, multiple ^{36}Cl/Cl peaks recorded at the other two sites in New Mexico make comparisons difficult. The ^{36}Cl/Cl peak was 0.4 m deeper at SNWR2 than at the Hueco Bolson, and the resultant moisture flux at SNWR2 (2.6 mm yr^{-1}) was almost twice that at the Hueco Bolson (1.4 mm yr^{-1}; Figure 17, Table A2). Although the ^{36}Cl-based moisture flux at the Yucca Wash site in Nevada (1.8 mm yr^{-1}) is similar to that recorded at the Hueco Bolson, the mean annual precipitation at the Nevada site (150 mm yr^{-1}) is approximately half that recorded at the Hueco Bolson (280 mm yr^{1}; Table A2). The percentage of mean annual precipitation that infiltrates was calculated by dividing the mean annual precipitation by the moisture flux and is higher at New Mexico (1.1 to 1.5%) and at Nevada (1.2%) than at the Hueco Bolson (0.5%); these differences may result from finer-grained surficial sediments at the Hueco Bolson (clay loam to loam) than at the other sites (sandy loam to fine sand; Table A2).

At two of the New Mexico sites and at the Hueco Bolson site, ^{3}H profiles consisted of three peaks [*Phillips et al.*, 1988]. The ^{3}H concentrations of the 1963–1964 peaks, however, were much greater at New Mexico (60 to 90 TU) than at the Hueco Bolson (28 TU; Table A2). Differences in ^{3}H peak concentrations may result from variations in ^{3}H input caused by differences in precipitation or evapotranspiration between the Hueco Bolson and New Mexico. A ^{3}H low that was estimated to occur in the 1972–1973 period was recorded at the New Mexico sites and at the Hueco Bolson. Deeper penetration of ^{3}H at SNWR1 (2.5 m) compared with that at NMSUR (1.4 m) and at the Hueco Bolson (1.4 m) was attributed to the predominance of coarser material at SNWR1 (see *Phillips et al.* [1988] and Table A2). Although the maximum penetration depths of ^{3}H vary from 1.4 to 2.5 m, the moisture fluxes at the two New Mexico sites are similar (8.4 to 9.5 mm yr^{-1}) because of lower moisture contents in the coarser-grained material. The ^{3}H data also indicate that the percentage of precipitation that infiltrates in New Mexico is almost twice that in the Hueco Bolson.

Moisture fluxes based on Cl and ^{3}H data agree well in humid regions such as South Australia (Cl moisture flux, 70 to 260 mm yr^{-1}; ^{3}H moisture flux 50 to 270 mm yr^{-1}) and Cyprus (Cl moisture flux, 49 to 51 mm yr^{-1}; ^{3}H moisture flux 48 mm yr^{-1}; Table A2) [*Allison and Hughes*, 1978; *Kitching et al.*, 1980]. In arid regions, such as parts of New Mexico and Texas, the moisture fluxes based on ^{3}H data (7.0 to 9.5 mm yr^{-1}) are much higher than those based on ^{36}Cl (1.4 to 3.0 mm yr^{-1}) and Cl (0.9 to 2.5 mm yr^{-1}) data. Faster transport of ^{3}H relative to ^{36}Cl or Cl in arid regions is attributed to ^{3}H transport in the vapor phase [*Phillips et al.*, 1988], whereas vapor transport is negligible in humid regions. Differences in moisture flux calculated from ^{3}H and ^{36}Cl data for New Mexico [*Phillips et al.*, 1988] suggest vapor fluxes that range from 5 to 7 mm yr^{-1}, which are consistent with vapor fluxes (2.5 to 10 mm yr^{-1}) calculated from profiles of oxygen and hydrogen stable isotopes for the same area [*Knowlton*, 1990]. These vapor flux estimates are similar to that calculated for the Hueco Bolson (6 mm yr^{-1}).

Comparisons among physical and chemical data from many of these sites are difficult because information on physical attributes of these regions is limited. Physical characteristics of the three New Mexico sites differ markedly. The water table is approximately 5 m deep at SNWR1 and measured water potentials are high (≥ -0.1 MPa), and the calculated moisture flux based on Darcy's law ranges from 7 to 37 mm yr^{-1} [*Stephens and Knowlton*, 1986]. In contrast, the water table is approximately 100 m deep at the other two sites in New Mexico, and measured water potentials range from -1 MPa at the surface to -5 MPa at 5-m depth at NMSUR (D. B. Hudson, personal communication, 1989). Despite the large difference in physical attributes at these sites, moisture fluxes based on chemical tracer data are remarkably similar (Cl moisture flux, 1.5 to 2.5 mm yr^{-1}; ^{36}Cl/Cl moisture flux, 2.5 to 3.0 mm yr^{-1}; ^{3}H moisture flux, 8.4 to 9.5 mm yr^{-1}) (Table A2). Water potentials are much lower at the Hueco Bolson (0 to -16 MPa) than at NMSUR (0 to -5 MPa), which indicates that the former system is much drier. Based on a comparison of the physical data, moisture fluxes also would be expected to be much lower in the Hueco Bolson than in New Mexico. Moisture fluxes based on ^{36}Cl data in the Hueco Bolson are approximately half those measured in New Mexico, whereas those based on ^{3}H data are similar in the two regions. The lack of general

correspondence between the hydraulic and chemical data may result partly because the chemical data record net moisture fluxes over a long time (≥30 years), compared with the short time of soil physics monitoring data (≤3 years).

CONCLUSIONS

Tritium penetrated much deeper than ^{36}Cl, although ^{3}H fallout occurred later than that of ^{36}Cl. Net downward fluxes estimated from the chemical tracers contrast with the upward driving forces for liquid water suggested by the water potential data. The discrepancy between the chemical and hydraulic data could be resolved if the tracers moved down by concentration-driven diffusion. Analysis of the ^{36}Cl profile suggests that diffusion alone cannot account for the distribution of ^{36}Cl, and advection is also involved. Downward percolation is episodic and is better estimated by long-term average fluxes from the chemical tracer data rather than by the limited time represented by the soil physics data.

Chlorine 36 is nonvolatile and is restricted to liquid-phase flow. The $^{36}Cl/Cl$ peak depth of 0.5 m yielded a moisture flux of 1.4 mm yr^{-1}. In contrast, tritiated water is volatile and can move in both liquid and vapor phases, and resulted in a moisture flux of 7 mm yr^{-1}. The higher moisture flux associated with ^{3}H relative to ^{36}Cl is attributed to enhanced downward movement of ^{3}H in the vapor phase. The difference in moisture fluxes between the two tracers suggests a vapor flux of approximately 6 mm yr^{-1}.

Nonisothermal liquid and vapor flow simulations for the summer and winter periods using the computer code SPLaSHWaTr showed large upward isothermal vapor fluxes during the day and small isothermal vapor fluxes at night. Thermal vapor fluxes were downward during the day and upward at night for both winter and summer. Net vapor flux was also downward during the day and upward at night. Total vapor fluxes were two to eight orders of magnitude greater than liquid fluxes for the periods simulated. Net vapor flux in the 5-day simulation period was upward in the top 0.04 m of the unsaturated zone in response to steep water potential gradients during the summer and winter. Downward summer vapor fluxes were much greater than winter vapor fluxes from 0.15- to 1-m depth, and suggest a net downward vapor flux on an annual basis that is consistent with the chemical tracer results.

Acknowledgments. This project was funded by the Texas Low-Level Radioactive Waste Disposal Authority under contract IAC (88-89) 0932. Soil samples for ^{36}Cl analysis were collected by B. C. Richter, and analyses were conducted at the University of Rochester by P. W. Kubik and P. Sharma. Meteorologic data were provided by S. W. Lyons, P. C. D. Milly helped with use of the computer code SPLaSHWaTr. The author benefited from many discussions with D. R. Hampton and F. M. Phillips, and A. R. Dutton provided helpful review. T. F. Hentz was technical editor. Word processing was by M. Snell, and drafting by J. Jobst under the direction of R. L. Dillon.

REFERENCES

Allison, G. B., and M. W. Hughes, The use of environmental chloride and tritium to estimate total recharge to an unconfined aquifer, *Aust. J. Soil Res.*, *16*, 181–195, 1978.

Allison, G. B., W. J. Stone, and M. W. Hughes, Recharge in karst and dune elements of a semi-arid landscape as indicated by natural isotopes and chloride, *J. Hydrol.*, *76*, 1–26, 1985.

Bentley, H. W., F. M. Phillips, and S. N. Davis, ^{36}Cl in the terrestrial environment, in *Handbook of Environmental Isotope Geochemistry*, vol. *2b*, edited by P. Fritz and J.-C. Fontes, pp. 422–475, Elsevier Science, New York, 1986.

Biggar, J. W., and D. R. Nielsen, Miscible displacement, II, Behavior of tracers, *Soil Sci. Soc. Am. Proc.*, *26*, 125–128, 1962.

Campbell, G. S., *Soil Physics With BASIC: Transport Models for Soil-Plant Systems*, 150 pp., Elsevier, New York, 1985.

Carslaw, H. S., and J. C. Jaeger, *Conduction of Heat in Solids*, 2nd ed., 510 pp., Oxford at the Clarendon, London, 1959.

Conca, J. L., and J. Wright, Aqueous diffusion coefficients in unsaturated materials, *Mater. Res. Soc. Symp. Proc. 212*, 879–884, 1991.

de Marsily, G., *Quantitative Hydrogeology*, 440 pp., Academic, San Diego, Calif., 1986.

de Vries, D. A., Thermal properties of soils, in *Physics of Plant Environment*, edited by W. R. van Wijk, pp. 210–235, North-Holland, Amsterdam, 1963.

Duval, T. A., Thermonuclear tritium as a tracer for liquid and vapor transport of soil moisture through arid soils, M.S. thesis, 81 pp., N. M. Inst. of Min. and Technol., Socorro, 1986.

Elmore, D., B. R. Fulton, M. R. Clover, J. R. Marsden, H. E. Gove, H. Naylor, K. H. Purser, L. R. Kilius, R. P. Beukens, and A. E. Litherland, Analysis of ^{36}Cl in environmental water samples using an electrostatic accelerator, *Nature*, *227*, 22–25, 1979.

Elmore, D., N. J. Conard, P. W. Kubik, and J. Fabryka-Martin, Computer controlled isotope ratio measurements and data analysis, *Nucl. Instrum. Methods Phys. Res., Sect. B*, *5*, 233–237, 1984.

Folk, R. L., *Petrology of Sedimentary Rocks*, 182 pp., Hemphill, Austin, Tex., 1974.

Gee, G. W., M. D. Campbell, J. H. Campbell, and G. S. Campbell, Rapid measurements of low soil water potentials using a water activity meter, *Agron. Abstr.*, 211, 1990.

Gvirtzman, H., D. Ronen, and M. Magaritz, Anion exclusion during transport through the unsaturated zone, *J. Hydrol.*, *87*, 267–283, 1986.

International Atomic Energy Agency (IAEA), Isotope techniques in the hydrogeological assessment of potential sites for the disposal of high-level radioactive wastes, *IAEA Tech. Rep. Ser. 228*, chap. 7, Vienna, 1983.

Jackson, R. D., B. A. Kimball, R. J. Reginato, and F. S. Nakayama, Diurnal soil-water evaporation: Time-depth-flux patterns, *Soil Sci. Soc. Am. Proc.*, *37*, 505–509, 1973.

James, R. V., and J. Rubin, Transport of chloride ion in a water-unsaturated soil exhibiting anion exclusion, *Soil Sci. Soc. Am. J.*, *50*, 1142–1149, 1986.

Kitching, R., W. M. Edmunds, T. R. Shearer, N. R. G. Walton, and J. Jacovides, Assessment of recharge to aquifers, *Bull. Sci. Hydrol.*, *25*, 217–235, 1980.

Knowlton, R. G., A stable isotope study of water and chloride movement in natural desert soils, Ph.D. dissertation, 241 pp., N. M. Inst. of Min. and Technol., Socorro, 1990.

Knowlton, R. G., F. M. Phillips, and A. R. Campbell, A stable-isotope investigation of vapor transport during ground-water recharge in New Mexico, *Rep. 237*, 88 pp., N. M. Water Resour. Res. Inst., Las Cruces, 1989.

Krupp, H. K., J. W. Biggar, and D. R. Nielsen, Relative flow rates of salt and water in soil, *Soil Sci. Soc. Am. Proc.*, *36*, 412–417, 1972.

Larkin, T. J., and G. W. Bomar, Climatic atlas of Texas, *Rep. TDWR LP192*, 151 pp., Tex. Dep. of Water Resour., Austin, 1983.

Mattick, J. L., T. A. Duval, and F. M. Phillips, Quantification of groundwater recharge rates in New Mexico using bomb ^{36}Cl, bomb ^{3}H and chloride as soil-water tracers, *Rep. 220*, 184 pp., N. M. Water Resour. Res. Inst., Las Cruces, 1987.

Milly, P. C. D., Moisture and heat transport in hysteretic, inhomogeneous porous media: A matric head–based formulation and a numerical model, *Water Resour. Res.*, *18*, 489–498, 1982.

Milly, P. C. D., A stimulation analysis of thermal effects on evaporation from soil, *Water Resour. Res.*, *20*, 1087–1098, 1984.

Milly, P. C. D., and P. S. Eagleson, The coupled transport of water and heat in a vertical soil column under atmospheric excitation, *Rep. 258*, 234 pp., Ralph M. Parsons Lab., Mass. Inst. of Technol., Cambridge, 1980.

Milly, P. C. D., and P. S. Eagleson, Parameterization of moisture

and heat fluxes across the land surface for use in atmospheric general circulation models, *Rep. 179*, 226 pp., Ralph M. Parsons Lab., Mass. Inst. of Technol. Cambridge, 1982.

Mualem, Y., A new model for predicting the hydraulic conductivity of unsaturated porous media, *Water Resour. Res.*, *12*, 513–521, 1976.

Nielsen, D. R., R. D. Jackson, J. W. Cary, and D. D. Evans (Eds.), *Soil Water*, pp. 131–138, American Society of Agronomy and Soil Science Society of America, Madison, Wis., 1972.

Nielsen, D. R., M. T. van Genuchten, and J. W. Biggar, Water flow and solute transport processes in the unsaturated zone, *Water Resour. Res.*, *22*, 89*S*–108*S*, 1986.

Norris, A. E., K. Wolfsberg, S. K. Gifford, H. W. Bentley, and D. Elmore, Infiltration at Yucca Mountain, Nevada, traced by ^{36}Cl, *Nucl. Instrum. Methods Phys. Res., Sect. B*, *29*, 376–379, 1987.

Philip, J. R., and D. A. de Vries, Moisture movement in porous materials under temperature gradients, *Eos Trans. AGU*, *38*, 222–232, 1957.

Phillips, F. M., J. L. Mattick, and T. A. Duval, Chlorine 36 and tritium from nuclear weapons fallout as tracers for long-term liquid and vapor movement in desert soils, *Water Resour. Res.*, *24*, 1877–1891, 1988.

Porter, L. K., W. D. Kemper, R. D. Jackson, and B. A. Stewart, Chloride diffusion in soils as influenced by moisture content, *Soil Sci. Soc. Am. Proc.*, *24*, 460–463, 1960.

Rose, C. W., Water transport in soil with a daily temperature wave, I, Theory and experiment, *Aust. J. Soil Res.*, *6*, 31–44, 1968*a*.

Rose, C. W., Water transport in soil with a daily temperature wave, II, Analysis, *Aust. J. Soil Res.*, *6*, 45–57, 1968*b*.

Scanlon, B. R., Evaluation of moisture flux from chloride data in desert soils, *J. Hydrol.*, *128*, 137–156, 1991.

Scanlon, B. R., P. W. Kubik, P. Sharma, B. C. Richter, and H. E. Gove, Bomb chlorine-36 analysis in the characterization of unsaturated flow at a proposed radioactive waste disposal facility, Chihuahuan Desert, Texas, *Nucl. Instrum. Methods Phys. Res.*, *52*, 489–492, 1990.

Scanlon, B. R., F. P. Wang, and B. C. Richter, Field studies and numerical modeling of unsaturated flow in the Chihuahuan Desert, Texas, *Rep. Invest. 199*, 55 pp., Bur. of Econ. Geol., Univ. of Tex., Austin, 1991.

Sophocleous, M., Analysis of water and heat flow in unsaturated-saturated porous media, *Water Resour. Res.*, *15*, 1195–1206, 1979.

Stephens, D. B., and R. Knowlton, Jr., Soil water movement and recharge through sand at a semiarid site in New Mexico, *Water Resour. Res.*, *22*, 881–889, 1986.

U.S. Department of Agriculture, *Soil Taxonomy*, 754 pp., Soil Conservation Service, Washington, D. C., 1975.

van de Pol, R. M., P. J. Wierenga, and D. R. Nielsen, Solute movement in a field soil, *Soil Sci. Soc. Am. J.*, *41*, 10–13, 1977.

van Genuchten, M. T., A closed-form equation for predicting the hydraulic conductivity of unsaturated soils, *Soil Sci. Soc. Am. J.*, *44*, 892–898, 1980.

van Genuchten, M. T., and W. J. Alves, Analytical solutions of the one-dimensional advection-dispersion solute transport equation, *Tech. Bull. 1661*, 151 pp., U.S. Dep. of Agric., Washington, D. C., 1982.

van Genuchten, M. T., and P. J. Wierenga, Mass transfer studies in sorbing porous media, II, Experimental evaluation with tritium, *Soil Sci. Soc. Am. J.*, *41*, 272–278, 1977.

Wierenga, P. J., and M. T. van Genuchten, Solute transport through small and large unsaturated soil columns, *Ground Water*, *27*, 35–42, 1989.

Wierenga, P. J., M. T. van Genuchten, and F. W. Boyle, Transfer of boron and tritiated water through sandstone, *J. Environ. Qual.*, *4*, 83–87, 1975.

Wilkinson, G. E., and A. Klute, The temperature effect on the equilibrium energy status of water held by porous media, *Soil Sci. Soc. Am. Proc.*, *26*, 326–329, 1962.

B. R. Scanlon, Bureau of Economic Geology, University of Texas at Austin, Austin, TX 78713.

(Received February 7, 1991;
revised August 20, 1991;
accepted August 22, 1991.)